Lattice Boltzmann Simulation of a Vortex Ring Impinging on a Sphere

Heng Ren*, Wanjun Liu, Lei Wang

Abstract— **Interaction of vortex rings with solid boundaries is an important research topic of hydrodynamic. In this study, a multiple-relaxation time (MRT) lattice Boltzmann method (LBM) is used to investigate the flow of a vortex ring impacting a sphere. The MRT-LBM is validated through the cases of vortex ring impacting a flat wall. The vortex evolution due to sphere size is discussed in detail. When the vortex ring impacting a stationary sphere, the interaction is described as the following three stages. Firstly, the secondary vortex is generated as the stretching of boundary vorticity at the beginning of impacting. In the second stage, the primary and secondary vortices expand and shrink radically and will wrap around each other. Finally, the primary vortex ring will recover from the 'wheel hub' structure.**

Index Terms— **Lattice Boltzmann method, vortex ring, sphere.**

[1] INTRODUCTION

As one of the typical forms of vortex motion, vortex rings widely exist in nature and engineering. The interaction of vortex rings with solid or fluid boundaries is a fundamental problem in fluid dynamics and has received considerable attention. This subject is also associated with a variety of practical applications, such as vortex rings extinguishing gas and oil well fires [1], cavitated rings used for underwater drilling [2], and modeling the interaction between the downburst and the aircraft [3]. Moreover, the underlying flow phenomena and physical mechanisms are still unclear and are of great interest for detailed studies.

Vortex rings interacting with a flat wall has been extensively studied. These studies [4-9] showed that as the primary vortex ring moves gradually toward the wall, its rate of approach slows and its radius continues to increase; meanwhile, considerable secondary vorticity is generated on the surface. When the Reynolds number, based on the initial diameter and translational speed of the vortex ring, is larger than about 500, the secondary vorticity separates from the surface and interacts with the primary vortex ring resulting in the ring rebounding from the wall. Actually, these studies are mainly limited to relatively low Reynolds numbers, the highest Reynolds number in these studies is about 2840 [9]. The experimental study [9] has revealed that, beyond Re = 3000 for the interaction between a vortex ring and a flat wall, the primary vortex ring will no longer remain stable as it approaches the wall.

Comparing with the numerous studies of vortex rings impacting a wall, the work of the interaction between a vortex ring and a sphere is scarce. To the best of our knowledge, the following two works were carried out in the literature. One is the experimental study of a vortex ring impacting a moving sphere [10]. In the experiment, a neutrally buoyant sphere was free to move in response to the impulse delivered by a vortex ring in water. The other work is a numerical study of the vortex interaction with a stationary sphere [11] using the implicit fourth-order compact finite difference schemes for solving the flow with Re=2000. Sousa analyzed the vortex dynamics of the ring as it approached the sphere surface [11]. He identified that the boundary layer formed on the surface of the sphere undergoes separation to form a second vortex ring, which grow rapidly as it interact with the primary ring. However, most of the previous studies are restricted to a flat or a sphere. The physical mechanisms are still unclear and the effect of sphere's size effect on the evolution of the vortices have never been addressed in the literature.

[2] NUMERICAL METHOD AND THE COMPUTATIONAL MODEL

[3] MRT-LBM

The simplest lattice Boltzmann method is the Bhatnagar-Gross-Krook (BGK) model, which is based on an approximation of a single relaxation time [12]. Until the 1990s, the MRT lattice Boltzmann method was developed, which overcomes some obvious defects of the BGK model, such as fixed ratio between the kinematic and bulk viscosities, improved the numerical stability [13].

The reasons why we use the MRT-LBM are illustrated in the follows. First, the LBM method is easy to implement and parallelized for this incompressible flow. Second, compared to conventional Navier-Stokes solvers of equal order of accuracy, the LBM has relatively low numerical dissipation and dispersion.

There are only two main steps in the code: streaming and collision. In the streaming step, the Distribution Functions (DF) in different directions (e.g., there are 19 components in the D3Q19 velocity model) at a computational node would propagate to its neighbourhood. The collision step is implemented locally. With the DF streaming from the neighbourhood, the macroscopic variables can be calculated as the moments of the DF. The DF can be updated through the collision step. In the collision step, the multiple-relax-time model is used to ensure a better numerical stability.

In our study, the fluid flow is solved by the MRT-LBM.

Manuscript received Sep 15, 2014.

***Heng Ren**, China Electronics Technology Group Corporation No.38 Research Institute, Hefei, China, +86 18900518514.*

***Wanjun Liu**, China Electronics Technology Group Corporation No.38 Research Institute, Hefei, China.*

***Lei Wang**, School of Naval Architecture and Ocean Engineering, Huazhong University of Science and Technology, Wuhan, China.*

ISSN: 2278 – 7798

The following MRT lattice Boltzmann (LB) equation [13] is employed to solve the incompressible Navier-Stokes equations,

$$\left|f(\mathbf{x}+\mathbf{e}_i\Delta t, t+\Delta t)\right\rangle - \left|f(\mathbf{x},t)\right\rangle = -M^{-1}\mathbf{S}\left[\left|m(\mathbf{x},t)\right\rangle - \left|m^{(eq)}(\mathbf{x},t)\right\rangle\right] \quad (1)$$

where the Dirac notation of ket $|\cdot\rangle$ vectors symbolize the column vectors. The particle distribution function $|f(\boldsymbol{x}, t)\rangle$ has 19 components f_i with i = 0, 1, ..., 18 in our 3D simulations because the D3Q19 velocity model is used. $\mathbf{e}_i$ are the discrete velocities of the velocity model. The directions of the velocities are shown in Fig. 1(a), and for example, $\mathbf{e}_1$ can be written as $\mathbf{e}_1$ = (1, 0, 0)c. Here $c = \Delta x/\Delta t$ is the lattice speed, where Δx and Δt are the lattice spacing (1lu) and time step (1ts) in LB simulations, respectively.

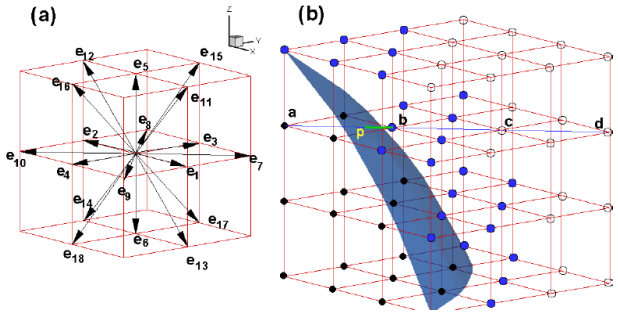

Fig. 1. (a) D3Q19 velocity model, $\mathbf{e}_1$ to $\mathbf{e}_{18}$ represent 18 non-zero components and $\mathbf{e}_0$ is a zero component and not labeled; (b) illustration of "interpolation bounce-back". The black filled circles are solid nodes, which are inside the surface of the solid body. The other circles are fluid nodes and the blue filled circles denote the fluid nodes which have at least one link with solid nodes (any of the 18 directions).

The collision matrix $\mathbf{S} = M \cdot S \cdot M^{-1}$ is diagonal with $\mathbf{S}$ [13],

$\mathbf{S} \equiv diag(0, s_1, s_2, 0, s_4, 0, s_4, 0, s_4, s_9, s_{10}, s_9, s_{10}, s_{13}, s_{13}, s_{13}, s_{16}, s_{16}, s_{16}) \cdot \left|m^{eq}\right\rangle$ is the equilibrium value of the moment $|m\rangle$. The 19 × 19 matrix M is a linear transformation which is used to map a vector $|f\rangle$ in discrete velocity space to a vector $|m\rangle$ in moment space, i.e., $|m\rangle = M \cdot |f\rangle$, $|f\rangle = M^{-1} \cdot |m\rangle$. The matrix M, the discrete velocities of the D3Q19 model, and $\left|m^{eq}\right\rangle$ are all identical as those used by [13].

The macro-variables density ρ and momentum j_ζ are obtained from

$$j_\zeta = \sum_i f_i, \qquad j_\zeta = \sum_i f_i e_i \zeta, \quad (2)$$

where ζ denotes x, y, or z coordinates. Here the collision process is executed in moment space [13]. In our simulations, the parameters are chosen as: $s_1 = 1.19$, $s_2 = s_{10} = 1.4$, $s_4 = 1.2$, $s_9 = 1/\tau$, $s_{13} = s_9$, and $s_{16} = 1.98$. The parameter τ is related to the kinematic viscosity of the fluid with $v_f = c_s^2(\tau - 0.5)\Delta t$ and $c_s = c/\sqrt{3}$. The pressure in the flow field can be obtained from the density via the equation of state $p = c_s^2 \rho$.

Macroscopically, (2) is able to recover the incompressible Navier-Stokes equation [13]. In the implementation to ensure the incompressibility condition, usually the velocity in the flow field should not exceed 0.1c.

[4] Boundary conditions

As we know, the non-slip boundary condition should be ensured in the particle's surface. Here, the non-slip boundary condition in our study is based on the scheme of Lallemand [14]. In Fig. 1(b), the computational domain was separated by a solid surface. Some lattice nodes which inside the surface are solid nodes (filled black circles) and the collision steps are not implemented in these nodes. Outside the surface, there are fluid nodes, which are represented by the filled blue circles and black circles. The filled blue circle denote the fluid nodes which have at least one link of the 18 directions (shown in Fig. 1(a)) connecting with the solid nodes. Usually the half-way bounce back is used to ensure the non-slip boundary condition. In Fig. 1(b), we can see that after streaming step, there are 6 directions are unknown for the lattice node **b**, i.e., $f_1(\mathbf{b}), f_3(\mathbf{b}), f_5(\mathbf{b}), f_7(\mathbf{b}), f_{15}(\mathbf{b}), f_{11}(\mathbf{b})$. For the half-way bounce back scheme (or simple bounce back), the unknown DF that comes from the solid node is set to be the DF in the reverse direction, which is already known. For example, $f_1(\mathbf{b}) = f_2(\mathbf{b})$.

Here a more accurate curve wall boundary condition [14] is applied. In the follows, an example about how to get $f_7(\mathbf{b})$ is illustrated in detail and the other DFs can be obtained in the similar way. In Fig. 1(b), suppose the line **ab** intersects with the solid surface at point **p**. |**bp**| denotes the length of the green line **bp**. After the streaming step, the unknown $f_7(\mathbf{b})$ can be obtained through a second-order interpolation from the surrounding points. More details about the "interpolation bounce back" can be found in [14].

[5] Computational model

In this work, the size of the computational domain was $H \times H \times L$ in the x, y, and z-directions, respectively, where $H = 12r_0$ and $L = 11r_0$. r_0 is the initial radius of the ring and is used as a characteristic length. As illustrated in Fig.2, the vortex ring and the elliptical sphere are initially placed at a distance $z = 9r_0$ and $z_0 = 7r_0$, respectively. The sphere is placed exactly under the vortex ring center and the line connecting the centers of the vortex ring and the particle is on the z— axis.

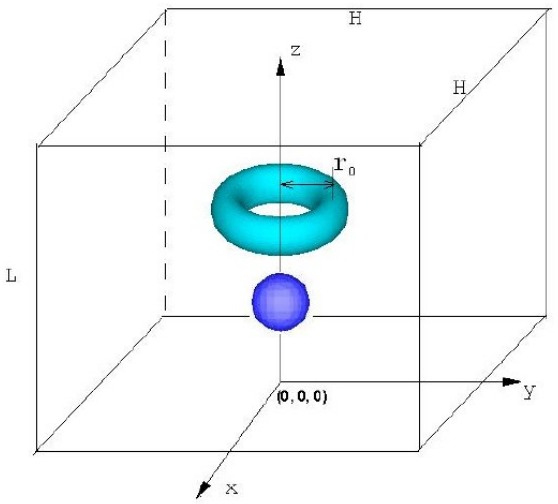

Fig. 2. Computation model for a vortex ring approaching a sphere.

ISSN: 2278 – 7798

The initial vorticity distribution of the vortex ring is assigned by a Gaussian function, i.e., the initial velocity field $\mathbf{u}_0 = (u, v, w)_0$ is specified as [4]

$$u_0 = \frac{\Gamma}{2\pi\sigma}\left[1 - e^{-(\sigma/\sigma_0)^2}\right]\boldsymbol{\theta}, \qquad (3)$$

where Γ is the circulation of the ring, $\boldsymbol{\theta}$ is the unit vector tangential to circulation circles of the vortex ring core, σ is the radial distance from the center of the core and the initial one is $\sigma_0 = \alpha r_0$. The corresponding initial translational speed of the vortex ring w_c is approximately [4]

$$w_c = \frac{\Gamma}{4\pi r_0}\left[\ln\frac{8r_0}{\sigma_0} - \frac{1}{4}\right]. \qquad (4)$$

In the simulation, constant-pressure boundary condition is applied on the six faces of the computational domain. For the boundary condition, the density of the fluid is specified as unity and the velocity is extrapolated from the inner fluid nodes. Then the equilibrium distribution function in the boundary fluid node can be calculated. The non-equilibrium part of the distribution function is extrapolated from the inner fluid nodes.

[6] Validation of the Numerical Method

To validate our code, grid-independence study was performed first. The vortex ring impacting a flat wall is simulated. As we know, some previous studies [4-8] demonstrate that for intermediate Re ($Re < 1000$), as long as H and $L \geqslant 10r_0$, the effect due to finite domain is negligible. Here, $H = 12r_0$ and $L = 11r_0$ are adopted. In the grid-independence study, four different meshes are used. The mesh resolutions are $r_0 = 20lu$, $25lu$, $30lu$, and $35lu$, respectively. The corresponding domain sizes in the simulations are $240\times240\times220$, $300\times300\times275$, $360\times360\times330$, $420\times420\times385$ respectively. In the simulations, the vortex ring is initially put $3r_0$ above the flat wall, $\alpha = 0.21$ and $Re = 830$.

Table 1. Peak value of the vorticity in the (y, z)-plane at dimensionless time T=10, 14, 18 for different meshes.

T	r_0=20	r_0=25	r_0=30	r_0=35
10	4.531	4.670	4.712	4.733
14	4.608	4.758	4.767	4.762
18	5.185	5.243	5.253	5.256

The peak values of vorticities in the (y, z)-plane at different times are compared and shown in Table 1. From Table 1, we can see that at the times listed, there are significant discrepancies between the case of $r_0 = 20lu$ and other cases (with maximum 3.2% discrepancy). On the other hand, the discrepancies between cases of r_0=30lu and r_0=35lu are much smaller (less than 0.3%) and negligible. The result shows that the grid with resolution r_0=30lu is fine enough to carry out relevant numerical study. Hence, in the following study, the mesh resolution is set to be r_0=30lu, i.e., the domain size is $360\times360\times330$.

To further validate our code, the trajectory of the primary vortex ring core is compared with the experimental data for the case $Re = 830$. The location of the primary vortex ($\bar{y}$, $\bar{z}$) is calculated through

$$\bar{y} = \frac{1}{\Gamma}\int_A y\omega_x dydz, \qquad \bar{z} = \frac{1}{\Gamma}\int_A z\omega_x dydz, \qquad (5)$$

where $A \in [0, H/2] \times L$ in the (y, z)– plane. As shown in Fig. 3, the LBM trajectory fits very well with the experiment data [8].

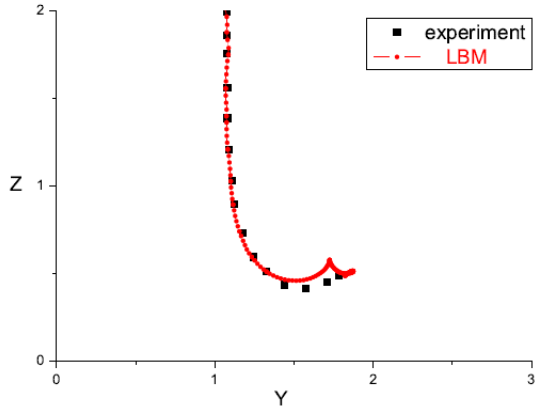

Fig. 3. The trajectory of the primary votex ring center for the case Re = 830. The line and squares denote our LBM result and the experimental data [8], respectively.

The evolution of the vortex is also compared with the experimental data and shown in Fig. 4. We can see the when the primary vortex ring approaches the flat wall, the secondary vortex is generated from the wall and rolls up ((b) and (c) in the figure). With the expansion of the primary vortex, the secondary vortex rolls up to the top of the primary vortex ((d) and (e)). Even the tertiary vortex structures can be seen in the last row of the figure.

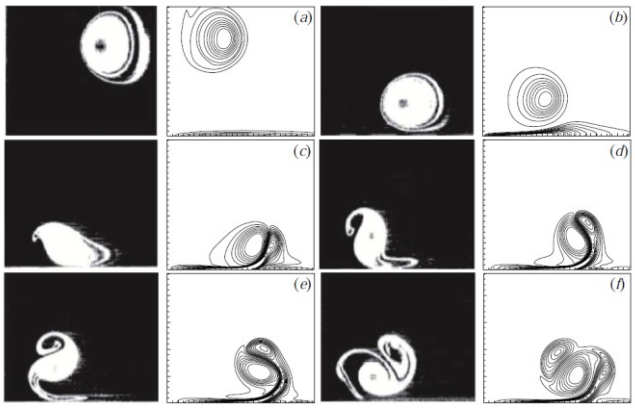

Fig. 4. The evolution of the vortex impacting a flat wall for Re = 830. The left and right columns are the experimental data [8] and our LBM result, respectively.

[7] Results and Discussion

In this section, the vortex ring impacting a sphere with different sphere size is studied. We focus on the dynamics of the flow, e.g., the evolution of the vortices. In the simulation, α is set to be 0.45, which means the primary vortex ring is thick.

Firstly, $r = 4/15\ r_0$ is investigated. Fig. 5 shows the evolution of the vortex ring for Re = 600. As shown in Fig. 5(1), when the vortex ring approaches the sphere, the intersection of the ring core is deformed to be an elliptical shape. Then, a very thin boundary layer is generated near the sphere (Fig. 5(2)). In Fig. 5(3), the boundary layer stretches

ISSN: 2278 – 7798

and it rapidly grows and separates from the spheroid. At the same time, the radius of the primary ring increases in response to the presence of sphere and the production of adverse pressure gradient at the solid wall [4]. As the interaction continues, the boundary layer rolls up from the sphere and forms a secondary vortex. Since these two vortex rings have opposite sign vorticity, the secondary vortex expands rapidly and the primary and secondary vortex rings wrap around each other. Figs. 5(4) and 5(5) show that the primary ring starts to decelerate considerably and the secondary vortex ring revolves as a satellite around the outside of the primary vortex core. Due to the secondary vortex, the primary ring was elongated and lost its elliptical form of the ring core and its radius does not increase as shown in Fig. 5(6). At this point, the primary ring stops its forward moving (the z-direction), while the remainder of the secondary vortex ring retains its link with the solid surface and may evolve a tertiary vortex but it is too weak to visualize [4]. As shown in Figs. 5(7) and 5(8), the elongated primary ring forms a 'wheel hub' structure and pinches off. The ring core changes to an elliptical shape again. Then, the primary ring restarts its forward motion and the radius reaches an approximately constant value. Finally, two distinct vortex rings are formed in Fig. 5(9). The primary ring continues its forward movement at a fixed velocity and the second ring is almost stationary around the sphere.

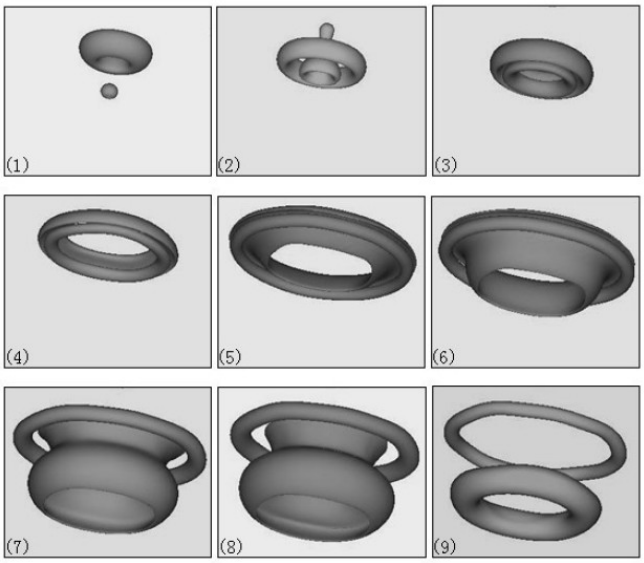

Fig. 5. Vortex structure evolution of the ring impacting a sphere for $Re = 600$ and the radius of the sphere is 4/15 r_0.

We explain why the second ring is almost stationary in the following. Obviously, the circulations of the secondary and the primary vortices are opposite, and the induced translational velocities are also opposite. On the other hand, the secondary vortex is weak and inside the velocity field dominated by the primary vortex. The induced upward translational velocity of the secondary vortex may be canceled by the downward velocity induced by the primary vortex. Hence, the secondary vortex may be stationary at that time interval we are interested in.

The evolution of the radius and translational velocity of the ring can be analyzed in detail in the follows. Fig. 6 shows the locations of x and z of the primary vortex ring, which were obtained by tracking the peak vorticity of the vortex center in the (x, z)— plane. It is seen that when the ring approaches the sphere, the velocity of the ring keeps constant and the displacement of x stays zero. As the ring goes closer to sphere, its radius begins to expand. During this time, the boundary layer starts to roll up and gradually lead to the secondary vorticity. At T=35, the primary ring nearly stops its forward motion. In this moment, the primary and secondary vortex rings wrap around each other. About the time of T=60, the primary ring pinches off. It restarts its forward motion with an elliptical ring core. The translational velocity is smaller compared to the initial speed. Finally, the ring moves with a constant velocity and its radius almost reaches a constant.

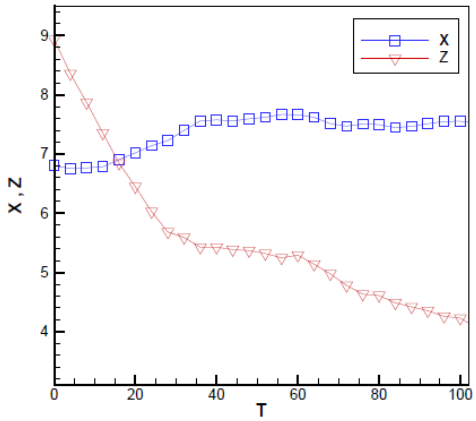

Fig. 6. Primary vortex ring location x and z as a function of time in the (x, z)-plane.

Cases of spheres with smaller radius $r = 1/6r_0$ and $1/15r_0$ are simulated. Fig. 7 shows the evolution of vortex rings with $r = 1/15\ r_0$ in the (x, z)-plane, which is qualitative similar to the behavior of the vortex rings in the case of $r = 4/15\ r_0$, except for the magnitude of vorticity.

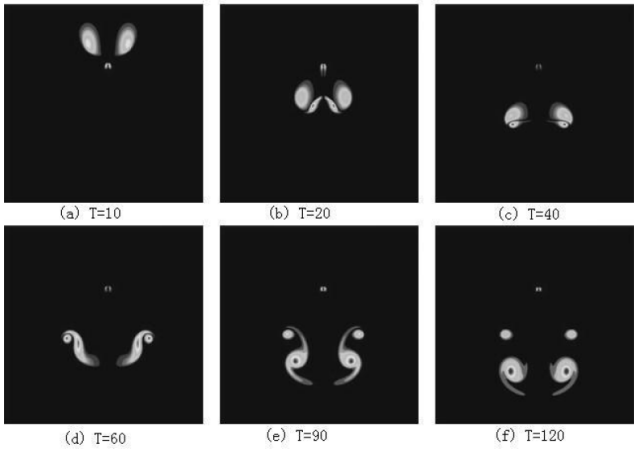

Fig. 7. The evolution of vortex impacting a small sphere in the (x, z)-plane.

Fig. 8 shows a quantitative comparison of the trajectories of the cases $r = 1/6\ r_0$ (open symbols) and $r = 4/15\ r_0$ (filled symbols). For the case of $1/6r_0$, the generated secondary vortex detaches from the sphere later than the case of 4/15 r_0. It seems the radius of the sphere would affect the final position of the secondary vortex. For a smaller sphere, the secondary vortex stays far away from the sphere. That is because when the sphere is large, the secondary vortex which is generated from the sphere experiences a stronger vortex

ISSN: 2278 – 7798

stretching.

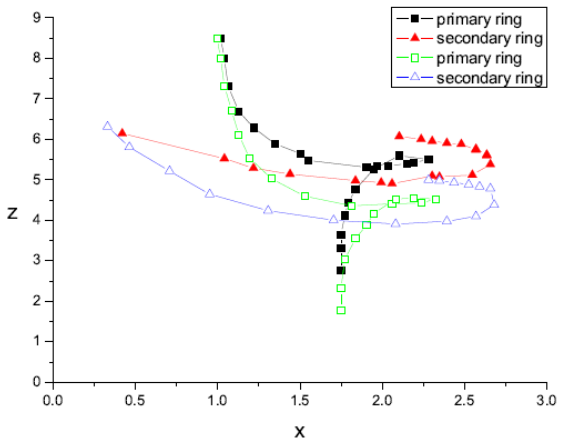

Fig. 8.The trajectory of the vortex rings impacting different spheres. Filled symbols represent the case of $r = 4/15\ r_0$ and open symbols represent the case of $r = 1/6\ r_0$.

[8] CONCLUSION

In this paper, a three-dimensional vortex ring impacting a sphere is studied using the MRT-LBM. The evolution of the vorticity on the symmetric planes, trajectories of vortex center and the effects of sphere size on the evolution of vortex structure are discussed in detail.

When the vortex ring impacting with a sphere, the interaction is described as the following three stages. Firstly, the secondary vortex is generated as the stretching of boundary vorticity at the beginning of impacting. In the second stage, the primary and secondary vortices expand and shrink radically and will wrap around each other. Finally, the primary vortex ring will recover from the wheel hub structure.

The trajectories of the primary and secondary vortices demonstrate that the wrapping pattern of primary and secondary vortex rings is very different from the situation of the vortex ring impacting a plate. The evolution of vortex structure seems sensitive to the size of the sphere. When the sphere is smaller, the primary ring expands slowly and eventually, the secondary vortex stays further from the sphere.

REFERENCES

[9] D. G. Akhmetov, B. A. Lugovtsov, and V. F. Tarasov, "Extinguishing gas and oil well fires by means of vortex rings," *Combust. Explos. Shock Waves*, vol. 16, pp. 490-494, 1980.

[10] G. L. Chahine, and P. F. Genoux, "Collapse of a cavitating vortex ring," *J. Fluid Eng.*, vol. 105, pp. 400-405, 1983.

[11] T. S. Lundgren, and N. N. Mansour, "Vortex ring bubbles," *J. Fluid Mech.*, vol. 224, pp. 177-196, 1991.

[12] M. Cheng, J. Lou, and L. S. Luo, "Numerical study of a vortex ring impacting a flat wall," *J. Fluid Mech.*, vol. 660, pp. 430-455, 2010.

[13] T. T. Lim, T. B. Nickels, and M. S. Chong, "A note on the cause of rebound in the head-on collision of a vortex ring with a wall," *Exp. Fluids.*, vol. 12, pp. 41-48, 1991.

[14] P. Orlandi, and R. Verzicco, "Vortex rings impinging on walls: axisymmetric and three dimensional simulations," *J. Fluid Mech.*, vol. 256, pp. 615-646, 1993.

[15] A. M. Naguib, and M. M. Koochesfahani, "On wall-pressure sources associated with the unsteady separation in a vortex-ring/wall interaction," *Phys. Fluids.*, vol. 16, pp. 2613-2622, 2004.

[16] C. C. Chu, C. T.Wang, and C. C. Chang, "A vortex ring impinging on a solid plane surface-Vortex structure and surface force," *Phys. Fluids A*, vol. 7, pp. 1391-1401, 1995.

[17] J. D. A. Walker, C. R. Smith, A. W. Cerra, and T. L. Doligalski, "The impact of a vortex ring on a wall," *J. Fluid Mech.*, vol. 181, pp. 99-140, 1987.

[18] J. J. Allen, Y. Jouanne, and B. N. Shashikanth, "Vortex interaction with a moving sphere," *J. Fluid Mech.*, vol. 587, pp. 337-346, 2007.

[19] P. J. F. de Sousa, "Three-dimensional instability on the interaction between a vortex and a stationary sphere," *Theor. Comput. Fluid Dyn.*, vol. 26, pp. 391-399, 2012.

[20] P. L. Bhatnagar, E. P. Gross, and M. Krookm, "A model for collision processes in gases. 1, Small amplitude processes in charged and neutral one-component systems," *Phys. Rev.*, vol. 94, pp. 511-525, 1954.

[21] D. Humieres, D. I. Ginzburg, M. Krafczyk, P. Lallemand, and L. S. Luo, "Multiplerelaxation-time lattice Boltzmann models in three dimensions," *Phil. Trans. Royal Society of London: Series A*, vol. 360, pp. 437-451, 2002.

[22] P. Lallemand, and L. S. Luo, "Lattice Boltzmann method for moving boundaries," *J. Comp. Physics*, vol. 184, pp. 406-421, 2003.

[23] Y. Chen, Q. D. Cai, Z. H. Xia, M. R. Wang, and S. Y. Chen, "Momentum-exchange method in lattice Boltzmann simulations of particle-fluid interactions," *Phys. Rev. E.*, vol. 88, 013303, 2013.

Heng Ren received B. E. degree in Engineering Mechanics from Lanzhou University and Ph. D degree in Engineering Mechanics from University of Science and Technology of China. Presently working as an engineer in China Electronics Technology Group Corporation No.38 Research Institute. His research areas are Computational Fluid Dynamics and Thermal physics.

Wanjun Liu working as an engineer in China Electronics Technology Group Corporation No.38 Research Institute. His research areas are Mechanic Design and Thermal physics.

Lei Wang received B. E. degree in Engineering Mechanics from Lanzhou University and Ph. D degree in Engineering Mechanics from University of Science and Technology of China. Presently working as a lecturer in School of Naval Architecture and Ocean Engineering, Huazhong University of Science and Technology. His research areas is Ship Mechanics.

ISSN: 2278 – 7798